Measurement Science
and Technology

Looseness detection system of bolted joints using a VMD-based nonlinear transformation approach with deep residual network

To cite this article before publication: DongYoon Kim *et al* 2025 *Meas. Sci. Technol.* in press https://doi.org/10.1088/1361-6501/ada821

Looseness detection system of bolted joints using a VMD-based nonlinear transformation approach with deep residual network

Dong-Yoon Kim[1], **Min-Je Kim**[1], **Chun-Il Kim**[2]‡, **Gil Ho Yoon**[1]§

[1] Department of Mechanical Engineering, Hanyang University, Seoul, South Korea

[2] Department of Mechanical Engineering, University of Alberta, Edmonton, Canada

E-mail: cikim@ualberta.ca and ghy@hanyang.ac.kr

July 2024

Abstract. Bolted structures are subject to various vibrations, external forces and environmental factors, all of which can reduce their structural stability and compromise the integrity of bolted connections. Detecting bolt loosening in advance is crucial, as these effects often cause bolts to become loose, potentially leading to structural failure or collapse. However, identifying looseness in complex or large structures poses significant challenges, particularly when there is insufficient prior information about the loose-fit condition. To address this issue, the present study proposes a novel detection system for bolted joint looseness, employing a Variational Mode Decomposition (VMD)-based Nonlinear Transformation (NT) approach integrated with a deep residual neural network, under several underlying assumptions. The proposed method utilizes VMD to decompose transverse vibrational modes into Intrinsic Mode Functions (IMFs), selectively extracting signals with desired modes. The NT method is then applied to scale and shift the extracted signals, transforming them into a form that facilitates approximate classification. Image-based spectrograms are generated from the differences between transformed and reference signals, which are subsequently analyzed by the deep residual network. To validate the proposed method, several plates with bolted joints are considered.

Keywords: bolted joint looseness, variational mode decomposition, nonlinear transformation, deep residual network, transverse vibration

Submitted to: *Meas. Sci. Technol.*

‡ Corresponding author 2

§ Corresponding author 1

1. Introduction

In most mechanical structures with bolted joints, various vibrations, external forces and environmental factors such as resonance effects, cyclic loading, abrasive wear and rust, can compromise the integrity of bolted connections, posing significant operational hazards. These factors often lead to the loosening of bolted joints, which can potentially result in structural failure or even collapse. Traditional approaches to addressing this issue have primarily relied on vibration-based methods to evaluate structural safety and predict faults, as proposed in various studies [1, 2, 3, 4, 5]. Additionally, artificial intelligence techniques have been integrated into health monitoring systems for bolted joints, enabling the detection of abnormalities through training on large datasets [6, 7, 8, 9]. However, identifying looseness in complex or large structures that are difficult to assess directly remains a significant challenge. This diagnostic approach is often limited by constraints in data collection and measurement, particularly when there is insufficient prior information about the loose-fit condition. To overcome these challenges, this study proposes a novel looseness detection system for bolted joints, employing a Variational Mode Decomposition (VMD)-based Nonlinear Transformation (NT) approach integrated with a deep residual network. In the VMD process, signals within the target frequency ranges are extracted by considering the mechanical characteristics of both simplified and complex systems. In the NT process, the vibration response of the complex system, with limited prior information, is interpreted by mapping it to the vibration response of the simplified system. After that, the looseness conditions of bolted structures are detected with the image-based spectrograms and deep residual network.

Vibration-based methods are widely used to diagnose structural abnormalities. Among these methods, research has focused on detecting damages using frequency response functions [10, 11, 12, 13, 14, 15, 16]. Detection assessment methods based on eigenfrequency data were presented in [17, 18, 19, 20], while structural damage detection techniques employing wavelet signals were explored in [21, 22]. Vibration analysis has also been applied to fault detection in wind turbines and the diagnosis of pump faults [23, 24, 25]. For bridge damage detection, vibration-based approaches were employed in [26, 27, 28]. Research on detection methods utilizing the cross-correlation functions of vibration responses was conducted in [29, 30]. Empirical mode decomposition techniques, which directly extract modes, have been employed to identify abnormal conditions in [31, 32]. Additionally, VMD methods, recognized for their advantages in signal decomposition within the frequency domain, have been utilized for fault diagnosis [33, 34, 35, 36]. Fault detection in rotating machinery was achieved by integrating the VMD with multiscale singular value decomposition [37]. To monitor the conditions of the transmission tower, a method for extracting the free vibration response was employed in [38]. Furthermore, focusing on various methods of data preprocessing, fault feature extraction and identification, a review of studies on vibration-based fault detection in rolling bearings was presented in [39].

To investigate the looseness of bolted joints, various vibration-based detection methods have been widely researched. Modal-based vibrothermography has been proposed to monitor the health conditions of bolted joints [40]. Diagnosis of bolt loosening has also been performed using laser excitation tests [41], while the looseness of bolted connections in pipelines was detected through changes in natural frequencies [42]. Additionally, a detection method employing an empirical mode decomposition-based nonlinear identification approach was proposed in [43]. Although vibration-based methods are effective for detecting abnormalities in bolted joints, alternative approaches have also been studied. For instance, ultrasonic wave-based techniques were employed to assess the conditions of bolted joints in [44, 45, 46]. To evaluate the quantitative health monitoring of bolted joints, a piezoceramic actuator-sensor was used in [47, 48]. Moreover, an acoustic health monitoring approach was presented to investigate the looseness in [49, 50]. An impedance-based structural health monitoring method was also presented in [51], and an active detection approach for loose bolts in complex satellite structures was studied in [52]. The detection method for looseness in bolted structures was developed by incorporating both direct and indirect measurement methods for axial force [53]. The locations of loose bolts and the axial forces of all bolts were predicted through tensile tests under different preload conditions [54]. Additionally, a classification method for bolt loosening based on wave energy dissipation using piezoelectric active sensing was explored in [55]. A monitoring method combining the inversion of magnetic field changes with surface clearance was proposed to detect bolt loosening [56].

Deep learning models are powerful tools for automatically diagnosing abnormalities, and image-based classification has been extensively studied. Among these models, supervised learning-based Convolutional Neural Networks (CNNs) have been widely researched for fault detection in various applications [57, 58, 59, 60]. Additionally, CNNs have been applied in the medical field for diagnosing diseases or specific parts [61, 62]. CNN models are known for their ability to classify objects quickly and accurately compared to other methods. However, many studies have explored diagnosing abnormalities using not only supervised learning but also unsupervised learning, semi-supervised learning, and reinforcement learning. A novel unsupervised model was developed for intelligent fault diagnosis in rotating machinery [63]. Semi-supervised learning using a stacked autoencoder was employed for fracture identification [64]. The reinforcement learning methods have been also utilized for intelligent fault detection, as demonstrated in [65, 66]. In addition, studies on fault detection using graph neural networks, which can learn relationships between nodes, edges and graph features, have been conducted in [67, 68].

The present study aims to detect the looseness of complex or large bolted joints using the VMD-based NT approach integrated with a deep residual network, as illustrated in figure 1. To execute the overall procedure, it is assumed that easily obtainable vibration signals from small structures with tight-fit and loose-fit conditions, as well as from large structures with tight-fit conditions, are known in advance. The process begins with the decomposition of the measured vibration signals through the VMD process, followed by the extraction of the desired mode. The extracted signals are then approximately classified using the nonlinear transformation method and the transformed signals are generated into virtual spectrograms with the difference between the signals. These virtual spectrograms are subsequently analyzed and diagnosed using the deep residual network.

This paper is organized as follows. Section 2 outlines the methodologies for detecting looseness in bolted joints. Section 3 demonstrates the validation of the proposed method through several examples. Section 4 concludes the study and offers suggestions for future research directions.

2. Methodology for detection of bolted joint looseness

2.1. Simplified lab-scale bolted joints versus complex large-scale bolted joints

This subsection outlines the assumptions made for detecting the vibration responses of complex and large-scale bolted joints using the vibration responses of simplified lab-scale bolted joints. It is assumed that vibration responses from simplified lab-scale bolted structures can easily be obtained and can be measured under both tight-fit and loose-fit conditions. These simplified structures allow for the assessment without difficulty under some different materials, boundary conditions and various factors that influence these responses. For complex and large-scale bolted structures, it is assumed that only the vibration responses of the tight-fit condition are known in prior. Whether produced as a finished product in a factory or assembled at a construction site, the vibration data of the tight-fit conditions of complex and large-scale bolted structures can be known in advance. However, the vibration responses under loose-fit conditions in complex structures are assumed to be unknown. In practice, conducting experiments or simulations on mega or geometrically complicated structures is both time-consuming and challenging, and detecting looseness conditions further increases the difficulty. The above assumptions are summarized as follows:

- **Assumption 1:** The vibration responses of the *tight-fit* and the *loose-fit* conditions of simplified or small reference bolted joints can be easily obtained.
- **Assumption 2:** The responses of the *tight-fit* conditions of complex or large bolted joints can be also obtained.
- **Assumption 3:** The responses of complex or large bolted joints with *loose fit* are difficult to be obtained.

Based on these three assumptions, this study aims to detect the loose-fit conditions of complex and large-scale bolted joints. To achieve this, vibration responses are measured using an acceleration sensor and an impact hammer. The process of approximating the responses between simplified reference and complex structures is performed on the obtained vibration data using variational mode decomposition (VMD) and nonlinear transformation (NT) methods. In the VMD process, the signal is decomposed around a target frequency where modes and peaks occur, and the intrinsic mode function (IMF) of the desired mode is extracted. The extracted signals are transformed into a frequency response function. Subsequently,

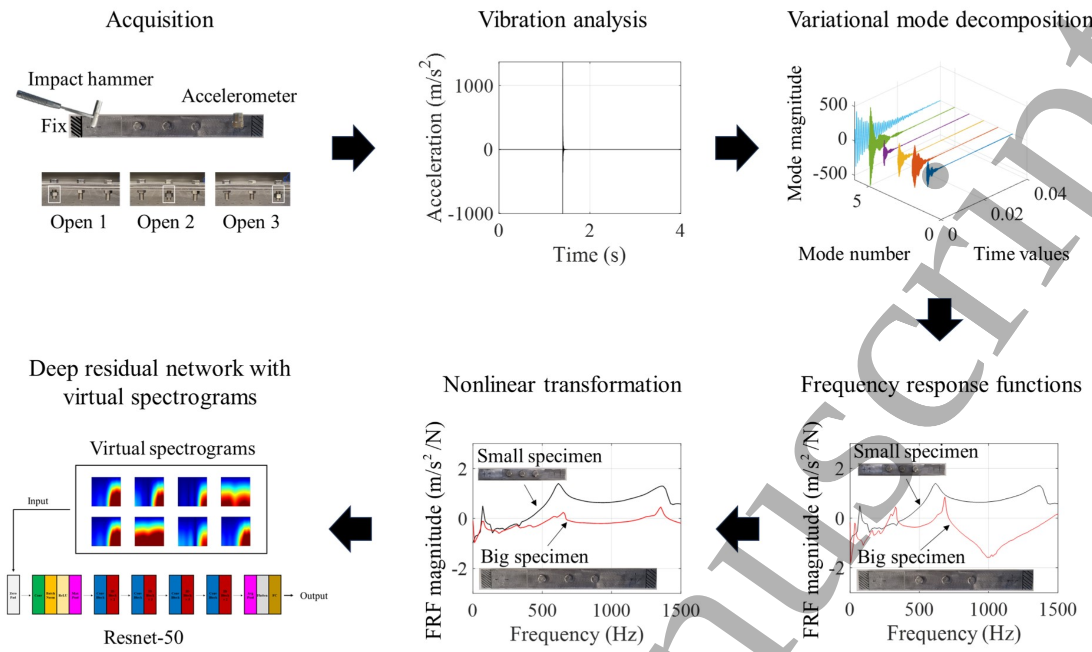

Figure 1. Procedure of the looseness detection system.

the NT method is applied between the frequency response functions, and these responses are converted into spectrogram images, which are then diagnosed using a deep residual network. The entire research procedure is illustrated in figure 1. This method enables the detection of differences even when there are geometrical, material, and bolt size discrepancies between the simplified and complex structures. In addition, this study is based on the fact that the eigenfrequencies associated with the order of mode shape appear similar from a mechanical engineering perspective with some differences in the geometry and material properties. It is acknowledged that the mode crossing phenomena may occur due to the differences in the material properties and the geometry.

2.2. Variational mode decomposition (VMD) of transverse vibration responses

This research utilizes the Variational Mode Decomposition (VMD) method to decompose the vibration signals [69, 70, 71]. Vibration modes contain valuable information about the mechanical characteristics of a system. Therefore, separating a vibration signal into individual modes facilitates a better understanding and estimating of the system's dynamic behavior. Within the framework of the VMD method, the proposed approach involves decomposing a vibration signal into individual components known as Intrinsic Mode Functions (IMFs). Each component exhibits distinct sparsity properties in the frequency domain [69]. A key feature of the VMD method is that each mode possesses a limited bandwidth and is primarily defined around a center frequency.

The IMFs are defined as amplitude-modulated-frequency-modulated signals as follows:

$$u_k(t) = A_k(t)\cos(\phi_k(t)) \tag{1}$$

where the phase and envelope are denoted by $\phi_k(t)$ and $A_k(t)$, respectively. The instantaneous frequency is denoted by $\omega_k(t) = \partial\phi_k(t)/\partial t$ in the k-th IMF. The detailed theoretical background of the VMD method can be referred to [69]. In the present study, the VMD is employed to decompose the acceleration signal into several IMFs, which are utilized for modal identification. This process is presented as a constrained variational problem as follows:

$$\min_{\{u_k\},\{\omega_k\}} \left\{ \sum_{k=1}^{K} \left\| \partial_t \left[\left(\delta(t) + \frac{j}{\pi t} \right) * u_k(t) \right] e^{-j\omega_k t} \right\|_2^2 \right\}$$
$$\text{subjected to } \sum_{k=1}^{K} u_k(t) = \ddot{x}_p(t) \tag{2}$$

where the Dirac function and convolution are denoted by δ and $*$, respectively. u_k and ω_k are the modes and center frequencies. With Lagrangian multipliers λ, the constrained variational problem can be transferred into an unconstrained optimization problem as follows:

$$L(\{u_k\},\{\bar{\omega}_k\},\lambda)=\alpha\sum_{k=1}^{K}\left\|\partial_t\left[\left(\delta(t)+\frac{j}{\pi t}\right)*u_k(t)\right]e^{-j\bar{\omega}_k t}\right\|_2^2+\left\|\ddot{x}_p(t)-\sum_{k=1}^{K}u_k(t)\right\|_2^2+\left\langle\lambda(t),\ddot{x}_p(t)-\sum_{k=1}^{K}u_k(t)\right\rangle \tag{3}$$

where α denotes the regularization parameter and it depends on the data fidelity constraint. The quadratic penalty term is considered to noise effect and Lagrangian multipliers are employed to utilize constraints. The alternate direction method is used to solve (3). With iterative sub-optimizations, the different center frequencies and modes are able to be obtained. Each mode is presented as:

$$u_k(\omega)=\frac{\ddot{x}_p(\omega)-\sum_{i\neq k}u_i(\omega)+(\lambda(\omega)/2)}{1+2\alpha(\omega-\bar{\omega}_k)^2}\quad(k=1,2,...,K) \tag{4}$$

where $\ddot{x}_p(\omega)$ is the fast Fourier transform (FFT) of the signal $\ddot{x}_p(t)$.

To perform the VMD method, several processes are proposed. The mode $u_k(\omega)$ is updated with (5). With a filter tuned to the center frequency $\omega_(k)$, Wiener filtering is applied for updating the mode.

$$u_k^{n+1}(\omega)=\frac{\ddot{x}_p(\omega)-\sum_{i<k}u_i^{n+1}(\omega)-\sum_{i>k}u_i^{n}(\omega)+(\lambda(\omega)/2)}{1+2\alpha(\omega-\bar{\omega}_k)^2}\quad(k=1,2,...,K) \tag{5}$$

In (6), the center frequency $\bar{\omega}_k^{n+1}$ is updated as follows:

$$\bar{\omega}_k^{n+1}=\frac{\int_0^\infty\omega\left|u_k^{n+1}(\omega)\right|^2d\omega}{\int_0^\infty\left|u_k^{n+1}(\omega)\right|d\omega} \tag{6}$$

All frequencies satisfy $\omega\geq 0$ and the Lagrangian multiplier $\lambda^{n+1}(\omega)$ is obtained by (7).

$$\lambda^{n+1}(\omega)=\lambda^{n}(\omega)+\tau\left(\ddot{x}_p(\omega)-\sum_k u_k^{n+1}\right) \tag{7}$$

$$\sum_{k=1}^{K}\frac{\left\|u_k^{n+1}-u_k^{n}\right\|_2^2}{\left\|u_k^{n}\right\|_2^2}\leq\varepsilon \tag{8}$$

where τ is the parameter of noise tolerance and ε is the convergence criteria, respectively. The whole iteration is conducted as the dual ascent and is finished until the convergence criteria as shown in (8).

The present study selected specific IMFs for detecting the looseness of bolted joints during the VMD process. The criteria for selecting IMFs consider stiffness and mass differences between the simplified and complex systems. Each target frequency range is determined and selectively employed based on the center frequencies where the desired mode and corresponding peak are located. The selected IMFs are then mapped using a nonlinear transformation method, which involves shifting and scaling according to the peak frequency.

2.3. Nonlinear transformation with frequency response functions of the selected IMFs

This subsection describes the nonlinear transformation (NT) method, which can conduct preliminary classification before performing an image-based deep residual network. The NT method has been studied for diagnosing various abnormalities, such as failures and delaminations, as shown in [72, 73]. This method allows for the approximate classification of signals before performing the deep learning process and increases the accuracy of diagnosis. In this study, the NT method is first carried out with the responses of the simplified bolted joints with a tight fit and the complex bolted joints with a tight fit. The responses are the frequency response functions (FRFs) of the selected IMFs in the previous VMD process. The NT function matches the eigenfrequencies of the tight-fit condition in the complex structure to those of the tight-fit condition in the simplified reference structure. Additionally, the signal of the tight-fit condition in the complex structure to which this function is applied can approximate the curve slope to some extent with respect to the signal of the tight-fit condition in the simplified structure. After the mapping function between the tight-fit systems is defined, the same mapping function is applied to the responses of the unknown condition in the complex structure. Before defining the mapping function, the frequency response function is defined as follows:

$$\mathrm{Y}=\mathrm{H}(\omega) \tag{9}$$

where the Y, H and ω denote the frequency response, response function and angular velocity, respectively. The mapping function matches the peak frequencies of the tight-fit condition in the complex structure to those of the tight-fit condition in the simplified reference structure. Herein, these peak frequencies are applied by shifting angular speed. The amplitudes of FRFs are also mapped by shifting and scaling of amplitudes.

$$\tilde{\omega_{\mathrm{c}}}=\left(\frac{\mathrm{H_s^{-1}}(\mathrm{Y_{max}^s})}{\mathrm{H_c^{-1}}(\mathrm{Y_{max}^c})}\right)\cdot\omega_{\mathrm{c}} \tag{10}$$

$$\tilde{\mathrm{Y}_{\mathrm{c}}}=\left(\frac{\mathrm{Y_{max}^s}-\mathrm{Y_{min}^s}}{\mathrm{Y_{max}^c}-\mathrm{Y_{min}^c}}\right)\cdot\mathrm{Y_c} \tag{11}$$

where the $\mathrm{Y_c}$ and $\mathrm{H_c}$ are the frequency response and transfer function of the complex system, the $\mathrm{Y_s}$ and $\mathrm{H_s}$ are those of the simplified system, respectively. The maximum FRF values of the simplified reference and complex systems are denoted by $\mathrm{Y_{max}^s}$ and $\mathrm{Y_{max}^c}$. The minimum FRF values are also denoted by $\mathrm{Y_{min}^s}$

and Y^{c}_{min}, respectively. The ω_c denotes the resonance frequencies of the complex system.

The frequency response functions (FRFs) of the simplified structure with the tight fit and those of the complex structure with the tight fit are transformed using the previously defined mapping function. In other words, the FRF of the complex structure with the tight fit is scaled and shifted to target that of the simplified structure with the tight fit. This function is once again applied to the FRF of the complex unknown-fit system. Then, the condition of the complex structure with the unknown fit can subsequently be determined. If the complex structure with the unknown fit is in the tight-fit condition, its FRF will closely resemble that of the simplified structure with the tight fit. Conversely, if the complex structure is in the loose-fit condition, its FRF will differ from that of the simplified structure with the tight fit. Moreover, the transformed response of the complex structure with the loose fit may resemble the FRF of the simplified structure with the loose fit; however, the eigenfrequencies of the two signals may not match exactly and could exhibit slight differences. Additionally, the nonlinear transformation method offers a significant advantage; data augmentation through the application of the mapping function. For instance, data can be augmented by the number of products of multiple signals to the simplified reference signal. To implement this method, several procedures are proposed as follows:

(i) Nonlinear transformation of the tight-fit systems
  - The dynamic responses of the complex tight-fit system (TS) transform to those of the simplified reference tight-fit system (TRS) with a mapping function.
  - TS is transformed to a mapped tight-fit system (MTS) as it is mapped to the target eigenfrequency of TRS.

(ii) Applying the same function to the unknown-fit system
  - The response of the complex unknown-fit system (US) is transformed into a mapped unknown-fit system (MUS) by applying the same defined function.
  - After this process, MTS and MUS can be approximately compared and classified to the TRS and simplified reference loose-fit system (LRS).
  - If TS and TRS match, there is no need to use this method and if there is a difference between the two signals, this method can be used to distinguish them.

2.4. Deep residual neural network with virtual spectrograms

This subsection describes the method of using a deep residual neural network to detect the looseness of bolted joints with virtual spectrograms created by differences between vibration signals. This study adopts Resnet-50, a so-called deep residual neural network, to classify the conditions of the bolted joint structures. ResNet-50 is recognized as one of the leading artificial intelligence networks for image classification and has been shown to surpass human recognition capabilities in certain tasks [74]. This network is developed to address the vanishing gradient and exploding gradient issues that arise as the network depth increases [74, 75, 76]. Some key features are residual blocks and skip connections. Residual blocks aim to learn the residual or difference between the input and the desired output instead of trying to learn an underlying function directly. This approach facilitates the training of deep networks by mitigating vanishing gradient problems. Skip connections allow the gradient to be directly backpropagated to earlier layers which aids in training deeper networks. To utilize these advantages, we employ the deep residual neural network with the following architecture in figure 2 and the details in table 1. The present models are trained with a mini-batch size of 8, a max epoch of 50, a learning rate of 0.0001, a shuffle in every epoch, a method of stochastic gradient descent with momentum and an image resizing of 224 × 224 in MATLAB [77].

In order to construct the looseness detection system using the deep residual network, frequency response functions (FRFs) obtained from the variational mode decomposition and nonlinear transformation processes are employed. With the differences between these FRFs, virtual spectrograms are generated to create training and validation datasets using a Short-time Fourier transform (STFT). In the training set, the tight-fit signals of the simplified structure (TRS) serve as the reference signal. Virtual spectrograms are generated from the differences between the TRS and the transformed tight-fit signals of the complex model (MTS), as well as the loose-fit signals of the simplified model (LRS). For the validation set, the transformed tight-fit signal of the complex structure (MTS) is used as the reference signal. Virtual spectrograms are then created from the differences between the MTS and the TRS, as well as the transformed unknown signals of the complex structure (MUS). These virtual spectrogram images are used with a size of 256 × 256. In the first example, 100 training and 100 validation data are employed, and in the second example, 125 training and 125 validation data are also employed. Note that each data in the training and validation datasets are different and experimental data. By leveraging the methods described above and the present deep residual neural network, the vibration-based looseness detection system for bolted joints is developed.

Table 1. The residual network architecture in detail.

Layer Name	Layer Description	Output Shape
Input	$224 \times 224 \times 3$	224×224
Conv1	Convolution filter 7×7, Strides 2, Number of filter 64, ReLU, Batch normalization	112×112
Conv2_x	Max pooling filter 3×3, Strides 2, ReLU, Batch normalization $\begin{bmatrix} 1 \times 1, 64 \\ 3 \times 3, 64 \\ 1 \times 1, 256 \end{bmatrix} \times 3$	56×56
Conv3_x	ReLU, Batch normalization $\begin{bmatrix} 1 \times 1, 128 \\ 3 \times 3, 128 \\ 1 \times 1, 512 \end{bmatrix} \times 4$	28×28
Conv4_x	ReLU, Batch normalization $\begin{bmatrix} 1 \times 1, 256 \\ 3 \times 3, 256 \\ 1 \times 1, 1024 \end{bmatrix} \times 6$	14×14
Conv5_x	ReLU, Batch normalization $\begin{bmatrix} 1 \times 1, 512 \\ 3 \times 3, 512 \\ 1 \times 1, 2048 \end{bmatrix} \times 3$	7×7
	Average pool, 1000-d FC, Softmax	1×1

2.5. Experimental setup

To demonstrate the application of the proposed approach, experiments are conducted. An impact hammer experiment is conducted with several bolted specimens to obtain transverse vibration signals, as shown in figure 3. Detailed parameters of the bolted specimens are provided in table 2. In example 1, one end of the specimen is clamped, while in example 2, both ends are clamped. The tight-fit condition of the bolted joints means that it has been tightened with a torque wrench until a torque of 15 N·m is reached. On the other hand, the loose-fit condition means that the torque applied by the torque wrench is 0 N·m. Data acquisition is carried out with the NI-9234 data acquisition device (DAQ), the accelerometer (PCB Piezotronics model 352C33) and the impact hammer (PCB Piezotronics model 086C03). The measured acceleration data are utilized in the variational mode decomposition process, while both force and acceleration data are employed to generate the frequency response function.

3. Experimental examples

This section presents several examples to verify the detection of looseness locations in complex structures with bolted joints using the methodologies described above. In each case study, the four types of specimens, i.e., simplified specimens with tight-fit and loose-fit joints, and complex specimens with tight-fit and unknown-fit joints are considered. The variational mode decomposition (VMD) method is employed to extract intrinsic mode functions (IMFs) from the acceleration data. The extracted signals are then transformed into frequency response functions (FRFs). The nonlinear transformation (NT) is applied between the FRFs of the simplified and complex bolted structures. Virtual spectrograms are subsequently generated based on the differences between signals obtained from the NT process. With these virtual spectrograms, the locations of the looseness in the complex bolted structures are detected through the deep residual network.

3.1. Example 1: Beam models with three bolted joints

In the first example, beam models with three bolted joints are considered in figure 4. It is assumed that the vibration responses of the simplified specimens with tight-fit and loose-fit joints and the vibration response of the complex specimen with tight-fit joints are known prior. However, the vibration response of the complex specimen with loose-fit joints is unknown, and it is intended to find out the loosened positions among joints. First, a transverse vibration experiment is performed with the simplified and complex bolted joints in figure 5. Acceleration data are measured over a duration of 4 seconds and are used to obtain the impulse response. As shown in figure 5, it is intricate to identify the relationship between signals of the simplified and complex structures with only acceleration signals and detecting the location of the looseness in bolted joints is also challenging. For this reason, the present study adopts a method of decomposing and filtering signals by applying the VMD to acceleration signals.

Figure 6 shows the VMD process with a representative signal of the simplified specimen with tight-fit joints. Figure 6 (a) and (b) show the original acceleration signal of the simplified specimen with tight-fit joints and the corresponding IMFs obtained through the VMD method. Each mode represents different central frequencies and is decomposed to the IMFs according to the central frequencies. Figure 7 (a) and (b) show the six IMFs and their fast Fourier transforms, respectively. The VMD method is generally employed to filter out noise and identify key characteristics of the signal. In the present study, VMD is applied to extract and utilize the bases of the signal for generating FRFs. The criteria for extracting IMFs and selectively converting them to FRFs are set to target the frequency ranges at which the third mode appears in both simplified and complex specimens. Specifically, a frequency range of 1000 - 1500 Hz is chosen for the simplified specimens, while a range of 500 - 1000 Hz is selected for the complex specimens, with the IMFs present in those ranges being utilized. For this example, two IMFs are considered because the IMFs present in the

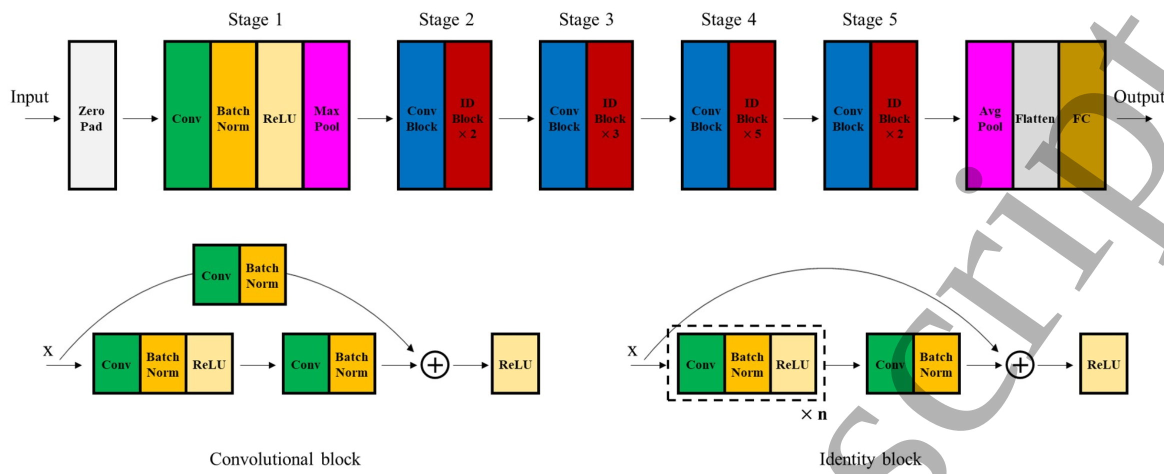

Figure 2. Residual neural network architecture.

Table 2. The detailed parameters of bolted joint specimens.

Specimen							Bolt		Nut	
Size	Case	Material	Width (mm)	Length (mm)	Thickness (mm)	Mass (g)	Diameter (mm)	Mass (g)	Diameter (mm)	Mass (g)
Small	Three holes	Stainless Steel	25	145	4.8	115	M8	12	M8	4
	Four holes	Structure Steel	67	154	4.8	378	M8	12	M8	4
Large	Three holes	Stainless Steel	38	250	5.6	394	M9	21	M9	6
	Four holes	Strcuture Steel	100	230	5.0	842	M12	42	M12	16

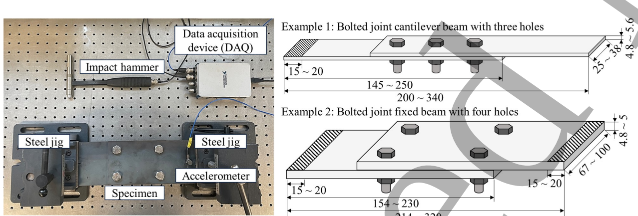

Figure 3. Vibration experimental setup.

target frequency ranges of the simplified and complex systems are different. Figure 8 (a) and (b) show the respective FRFs of the decomposed IMFs and the FRF generated by the fifth and sixth IMFs. These IMFs are represented in the frequency domain for use in the nonlinear transformation. With these FRFs, the nonlinear transformation process is carried out in the next process.

In the NT method, it is assumed that the vibration responses of simplified specimens with tight-fit and loose-fit joints and that of the complex specimen with tight-fit joints are known in advance. The goal of this approach is to approximately figure out the response of a complex specimen with loose-fit joints. To achieve this, the eigenfrequencies of the complex and simplified specimens with tight-fit joints are mapped. Figure 9 shows the application process of the nonlinear transformation method with a tight-fit reference signal (TRS) and loose-fit reference signal (LRS) of the simplified specimens, a tight-fit signal (TS) and an unknown-fit signal (US) of the complex specimens. Firstly, the vibration responses of TRS, LRS and TS are measured. Comparing the responses of the two tight-fit systems, a mapping function to fit the eigenfrequencies is able to be defined. In this example, the third mode of the TS is matched to that of the TRS. The function is defined considering the shifting factor of angular speed and the scaling and shifting factors of amplitudes. Here, the eigenfrequency of the third mode of the TS perfectly matches that of the TRS, and their slopes might become also similar. The overall dynamic responses of the system might become somewhat proportional as the responses are transformed. It is observed that the eigenfrequencies of a mapped tight-fit signal (MTS) of the complex specimen become similar to those of the TRS but differences in their magnitudes exist. Then, the unknown-fit signal (US) of the complex specimen is measured. The same mapping function is applied to the US, transforming it into a mapped unknown-fit signal (MUS). Finally, in the classification step, the eigenfrequencies of the MTS are roughly similar to those of the TRS and the system with the MUS might be similar to the system with the LRS.

Figure 10 shows the virtual spectrograms generated with the reference signals of the simplified specimens and the transformed signals of the complex specimens. The differences between these signals are transformed into virtual spectrograms using the Short time-Fourier transform. This process is applied to the TRS, LRS, MTS and MUS. An important consideration is the selection of reference data for calculating the differences. For the training dataset, virtual spectrograms are generated with TRS as the reference and are created by the difference between the MTS and TRS are designated as the TRS. Meanwhile, spectrograms constructed from the differences between the LRS 1, 2, 3, and TRS are labeled as LRS 1, 2 and 3, respectively. In the validation dataset, the MTS is selected as the reference data and the spectrograms generated by the difference between the TRS and MTS are denominated as a tight-fit condition. Spectrograms derived from the differences of the MUS and MTS are labeled as looseness conditions. The employed virtual spectrograms in the training and validation datasets show similarities. Utilizing these datasets, the locations of the looseness in complex bolted structures can be classified and diagnosed in the deep residual network.

Figure 11 (a) and (b) show the confusion matrices for looseness detection without and with the VMD-based NT method, and figure 12 (a) and (b) illustrate the corresponding confusion radar maps. Without the VMD-based NT method, locations of the LRS 1 are not detected, resulting in an overall detection accuracy of 70 %. On the other hand, with the present VMD-based NT method, the looseness of bolted joints is detected with a significantly improved accuracy of 95 %. As shown in figure 11 (b), the LRS 2, 3 and 4 in the validation dataset are detected with 100 % accuracy. On the other side, the looseness conditions of the LRS 1 are evaluated with an accuracy of 80 %. The discrepancy in detection accuracy for LRS 1 can be attributed to differences between the spectrograms of LRS 1 - TRS and MUS 1 - MTS. Although there are some errors, the locations of the looseness in complex bolted joints can be investigated with high accuracy. These findings emphasize the importance of the VMD-based NT method in detecting the conditions of complex bolted structures with simplified bolted structures. Thus, this example validates the effectiveness of the looseness detection approach with the VMD-based NT method.

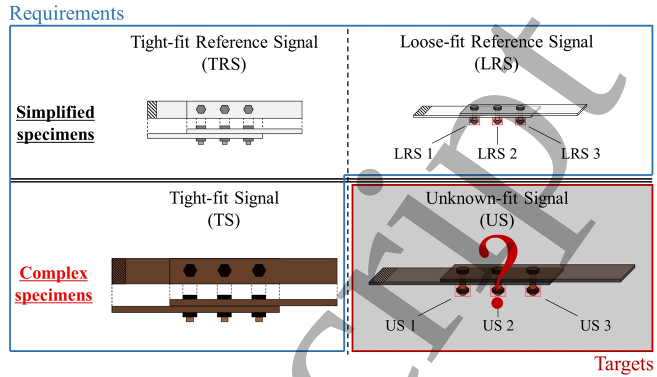

Figure 4. Illustration of geometric configurations represented by simplified and complex specimens with three bolted joints.

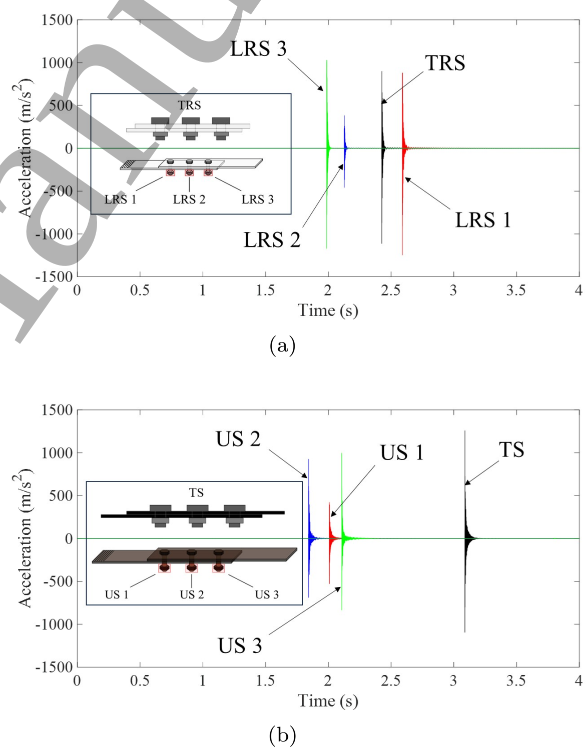

Figure 5. Acceleration data of the simplified and complex specimens measured by impact hammer for 4 seconds. (a) The acceleration signals of the four conditions of the simplified specimen with three bolted joints and (b) the acceleration signals of the four conditions of the complex specimen with three bolted joints.

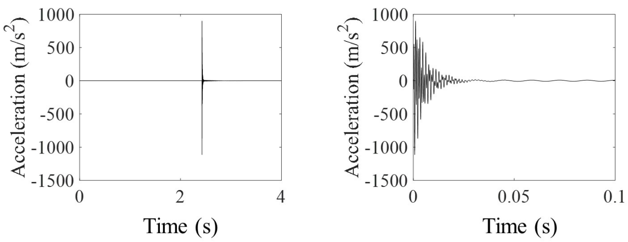

(a)

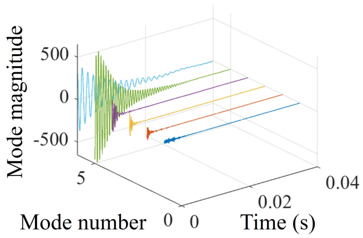

(b)

Figure 6. The VMD process with the acceleration signal of the representative simplified specimen with tight-fit joints. (a) The original acceleration signal and (b) the IMFs of the acceleration signal.

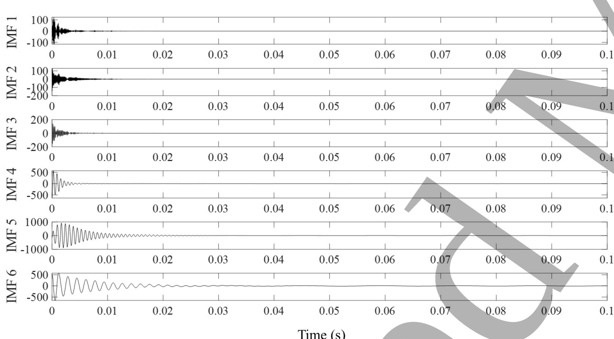

(a)

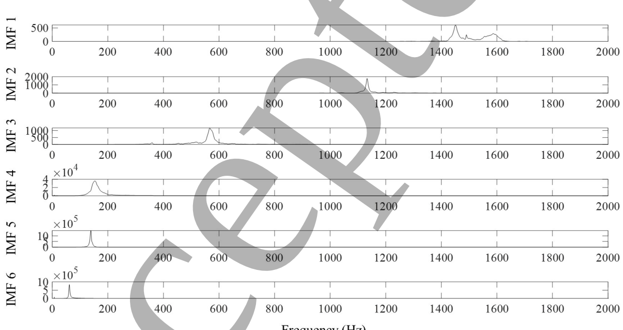

(b)

Figure 7. The IMFs generated with the acceleration signal of the tight-fit joints in the simplified specimen. (a) The IMFs of the acceleration signal and (b) the fast Fourier transformations of the IMFs.

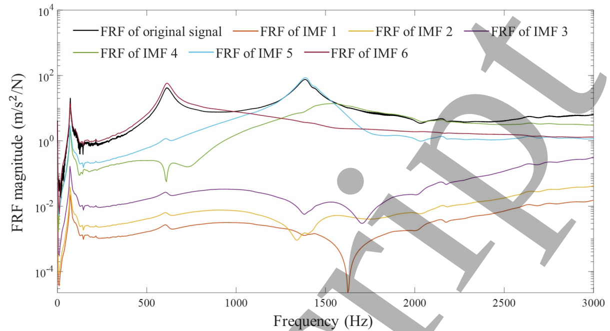

(a)

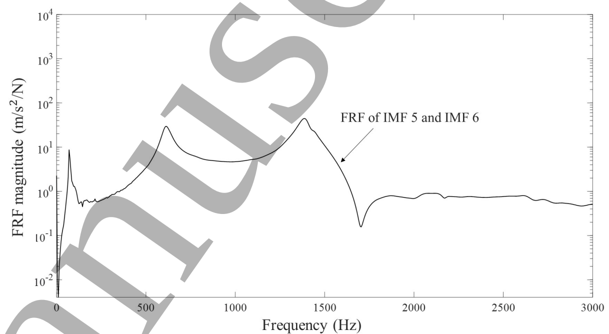

(b)

Figure 8. The FRFs constructed with the IMFs. (a) FRFs generated by the six IMFs and (b) the FRF generated by the IMF 5 and IMF 6.

3.2. Example 2: Beam models with four bolted joints

For the second illustrative example, the VMD-based NT method is applied to beams with four bolted joints that exist some types of mechanical looseness in figure 13. From a mechanical vibration perspective, the vibration response of the assembled structure is primarily determined by the vibration mode and resonance frequency, which depend on the stiffness and mass. The lighter mass of the bolt compared to the main mechanical structure has minimal impact on the vibration response, making it more challenging to identify and detect anomalies in bolted joints. In addition, the effects of the clamping forces of the bolts determining the stiffness values of the assembled structures are relatively small. For this reason, in this example, the vibration responses of the beams with the loose fit and the tight fit are hard to distinguish in the low-frequency range under 6000 Hz. Therefore, this example focuses on detecting loose-fit joints in large and complex specimens by analyzing the frequency range above 6000 Hz. It is important to note that the signals of all simplified specimens with tight-fit and loose-fit joints, as well as the signal of the complex specimen with tight-fit joints, are known in advance.

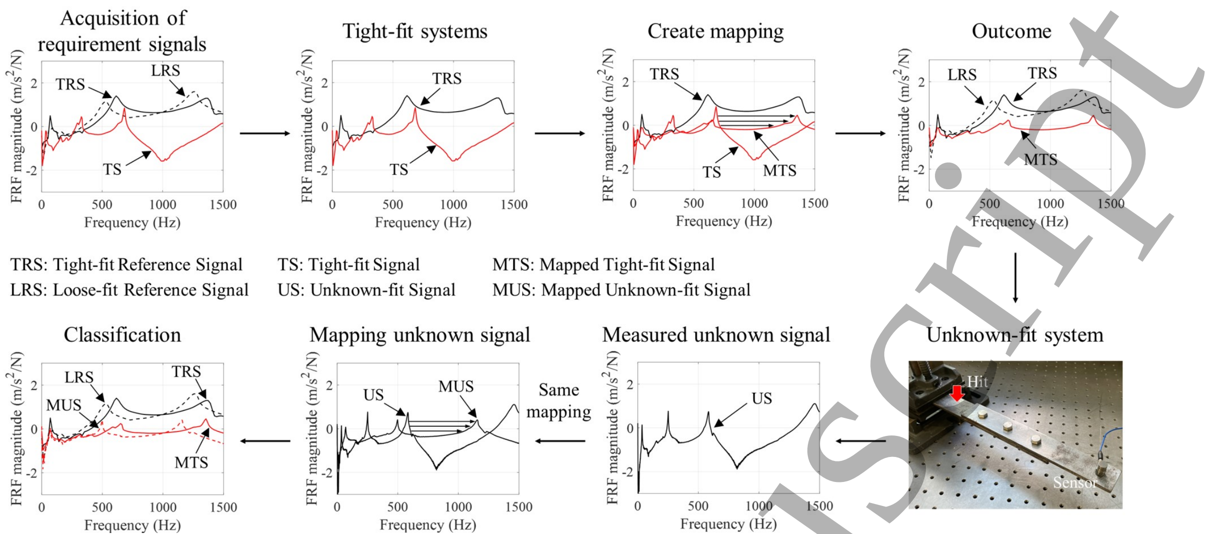

Figure 9. The NT process with the FRFs of the simplified and complex specimens with three bolted joints.

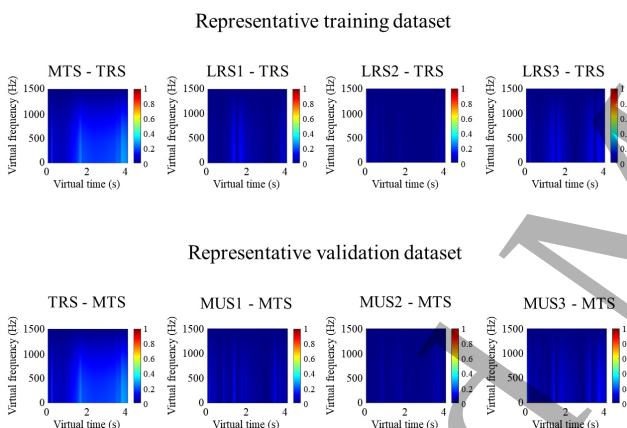

Figure 10. Representative virtual spectrograms created by the differences between the transformed signals and reference signals in the training and validation datasets.

First of all, acceleration signals of the assembled specimens are measured using a transverse vibration experiment, as depicted in figure 14. With these measured acceleration signals, the conditions of bolted joints are classified and detected through the VMD-based NT method combined with the deep residual network.

The VMD procedure for analyzing the acceleration signal of the representative simplified specimen with tight-fit joints is presented in figure 15. Figure 15(a) shows the original acceleration signal of the simplified specimen with tight-fit joints. Figure 15 (b) shows the intrinsic mode functions (IMFs) of the acceleration signal. With the above processes, figure 16 (a) and (b) show the six IMFs and their fast Fourier transformations. Comparing fast Fourier transformations, the acceleration signals of the representative simplified specimen with tight-fit joints can be seen decomposed into each mode and eigenfrequency. In this example, the target frequencies for the simplified and complex systems are approximately 7000 Hz and 3000 Hz, respectively. The third IMFs corresponding to the target frequency ranges are employed. Figure 17 (a) and (b) depict the FRFs of all IMFs and the FRF of the third IMF, respectively. Considering the eigenfrequencies of both the simplified and complex specimens, the FRF of the third IMF is used for the nonlinear transformation method.

Figure 18 shows the entire nonlinear transformation process with the representative tight-fit reference signal (TRS) and loose-fit reference signal (LRS) of the simplified specimens, and tight-fit signal (TS) and unknown-fit signal (US) of the complex specimens. In the acquisition step, the TRS, LRS and TS are measured. As previously discussed, a nonlinear mapping function is defined to approximately match the TS to the TRS. In the outcome step, the TRS, LRS and mapped tight-fit signal (MTS) of the complex specimen are presented. While the MTS does not completely match the TRS, their peak frequencies and slopes are able to be matched. Next, the US is measured and transformed using the previously defined mapping function, resulting in the mapped unknown-fit signal (MUS). Finally, in the classification step, the TRS, LRS, MTS and MUS can be identified. The TRS and MTS are observed to be similar, while the LRS and MUS exhibit differences from both the TRS and MTS. Through this process, the vibration signals can be approximately classified.

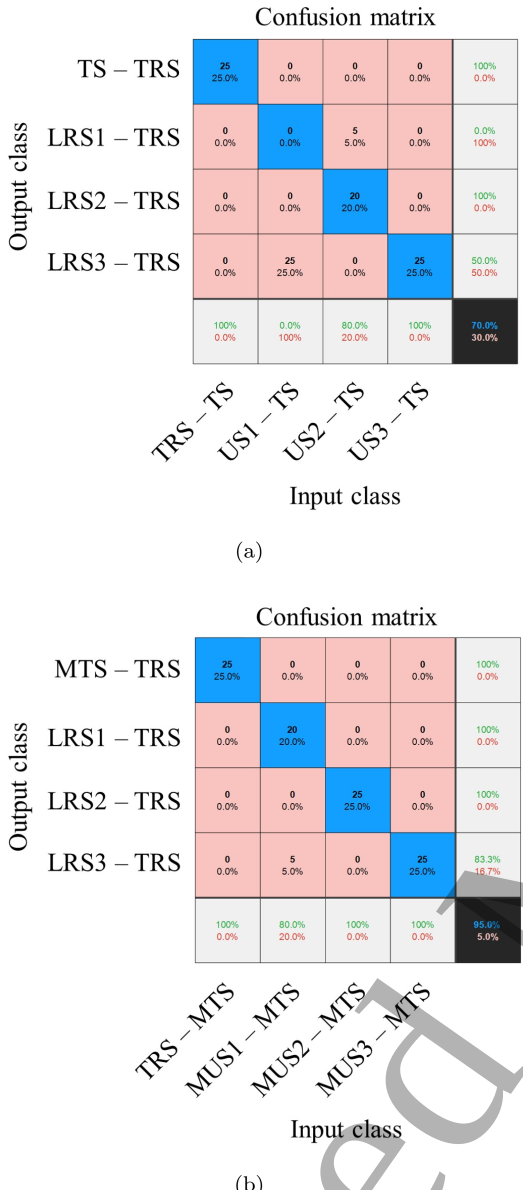

Figure 11. Confusion matrices showing the results of the looseness detection of the complex beam models with three holes. (a) The confusion matrix without the VMD-based NT method and (b) the confusion matrix with the VMD-based NT method.

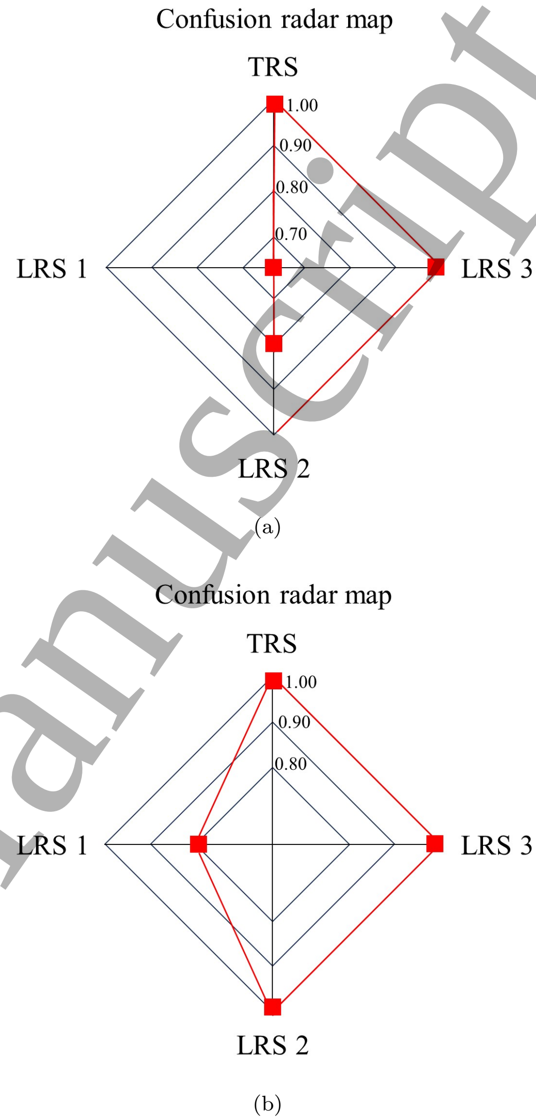

Figure 12. Confusion radar maps about the results of the confusion matrices. (a) The confusion radar map without the VMD-based NT method and (b) the confusion radar map with the VMD-based NT method.

Figure 19 shows representative virtual spectrograms generated by differences between the transformed FRF signals of the complex specimens and the reference FRF signals of the simplified specimens. In this example, the frequency range between 6800 and 7200 Hz is considered, as distinguishing differences in responses below 6000 Hz proves challenging. Similar to the previous example, the TRS in the training dataset and MTS in the validation dataset are designated as reference signals. In the training dataset, virtual spectrograms generated from the differences between the MTS and TRS are trained as the TRS condition, and those constructed with the differences between the LRS 1, 2, 3, 4 and TRS are trained as the LRS 1, 2, 3 and 4 conditions, respectively. For the validation dataset, virtual spectrograms generated from the differences between the TRS and MTS are evaluated by comparing them with the tight-fit condition of the training dataset, while those constructed from the differences between the MUS 1, 2, 3, 4 and MTS are assessed under looseness conditions. These virtual spectrograms are then used for the detection of looseness in complex bolted joints, utilizing the deep residual network for classification and diagnosis.

Figures 20 and 21 present the results of detecting the looseness of complex bolted joints with and without the VMD-based NT method. Without the VMD-based NT method, the locations of the LRS 1, 2 and 3 are not properly detected and the total results have an accuracy of 40 %. On the other side, the looseness detection of bolted joints using the VMD-based NT method is conducted with an accuracy of 92 %. As shown in figures 20 (b) and 21 (b), the virtual spectrograms corresponding to the MUS1 - MTS and MUS2 - MTS are detected as looseness conditions with an accuracy of 100 %. However, the spectrograms of the MUS3 - MTS and MUS4 - MTS are classified as looseness conditions with an accuracy of 80 %. Upon investigation, it is observed that the MUS3 - MTS, that is, some virtual spectrograms for the LRS 3 in the validation dataset resemble those of the LRS 2 in the training dataset. In addition, some virtual spectrograms of MUS4 - MTS are also detected with those of the LRS 2 in the training dataset. Despite these discrepancies, the results demonstrate that the VMD-based NT method significantly enhances the ability to accurately detect the locations of looseness in bolted joints compared to the method without VMD-based NT.

One of the attitudes is that it may be difficult to control the magnitudes when applying the VMD-based NT method. In addition, it can be difficult to investigate abnormalities in frequency bands higher than the frequency bands of the present study.

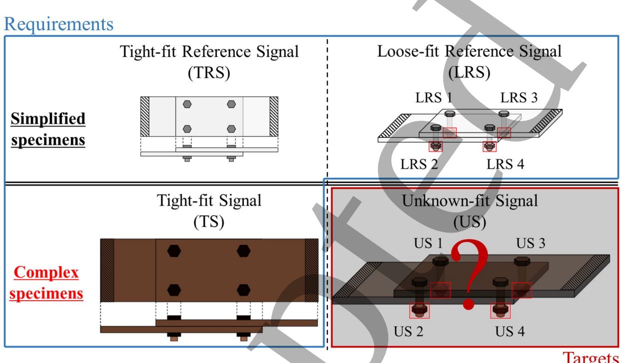

Figure 13. Illustration of geometric configurations represented by simplified and complex specimens with four bolted joints.

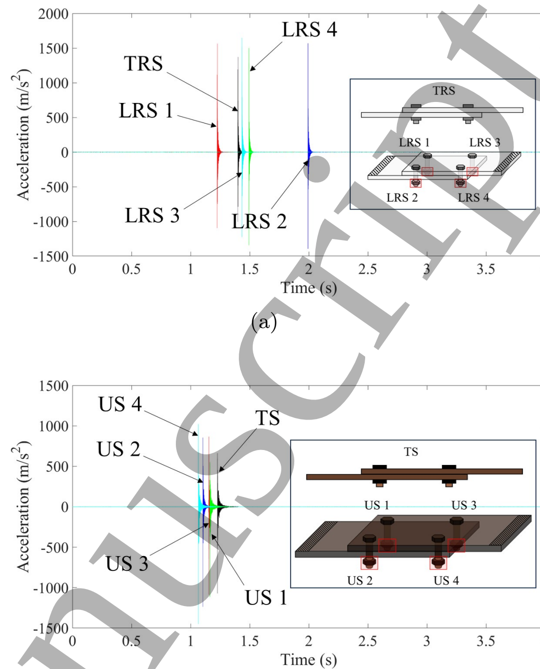

(a)

(b)

Figure 14. Acceleration data of the simplified and complex specimens measured by impact hammer for 4 seconds. (a) The acceleration signals of the five conditions of the simplified specimen with four bolted joints and (b) the acceleration signals of the five conditions of the complex specimen with four bolted joints.

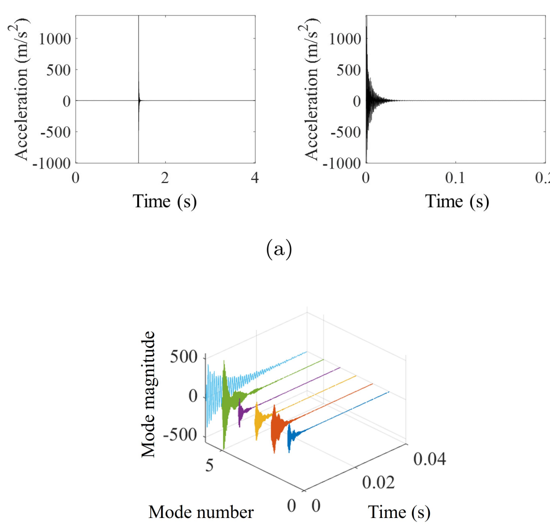

(a)

(b)

Figure 15. The VMD process with the acceleration signal of the representative simplified specimen with tight-fit joints. (a) The original acceleration signal and (b) the IMFs of the acceleration signal.

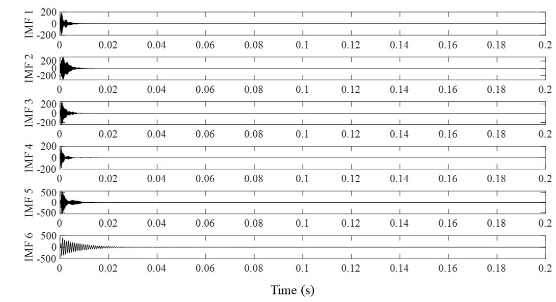

(a)

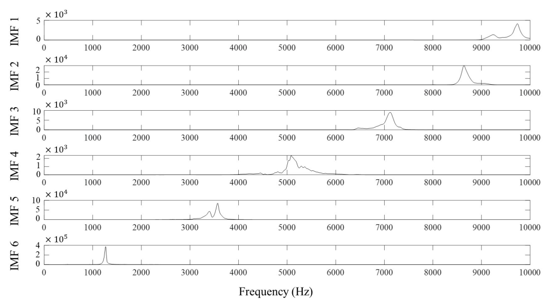

(b)

Figure 16. The IMFs generated with the acceleration signal of the tight-fit joints in the simplified specimen. (a) The IMFs of the acceleration signal and (b) the fast Fourier transformations of the IMFs.

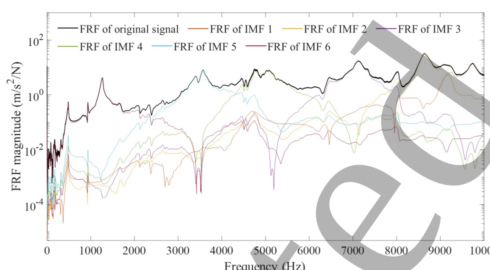

(a)

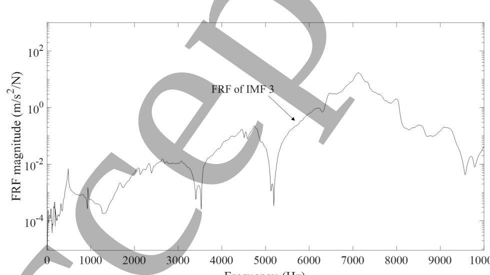

(b)

Figure 17. The FRFs constructed with the IMFs. (a) FRFs generated by the six IMFs and (b) the FRF generated by the IMF 3.

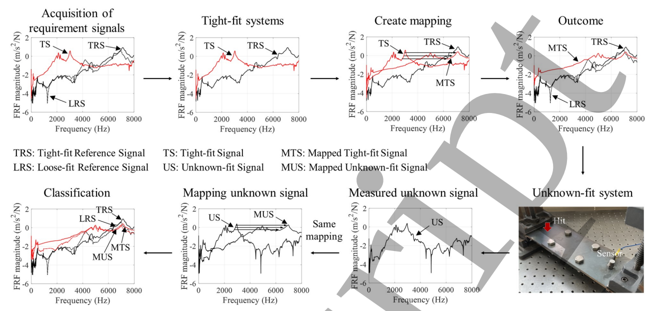

Figure 18. The NT process with the FRFs of the simplified and complex specimens with four bolted joints.

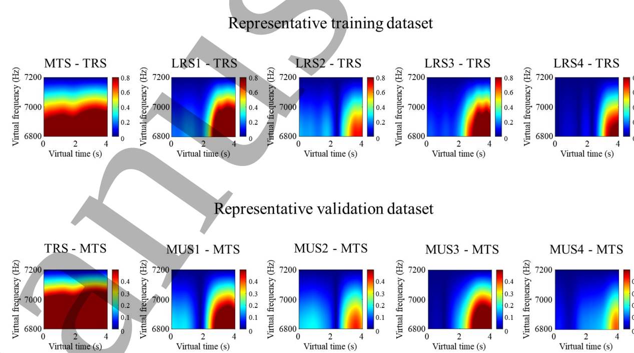

Figure 19. Representative virtual spectrograms created by the differences between the transformed signals and reference signals in the training and validation datasets.

4. Conclusion

This study proposes a novel detection system for bolted joint looseness using the Variational Mode Decomposition (VMD)-based Nonlinear Transformation (NT) approach integrated with the deep residual neural network, under certain assumptions. To verify the present method, several beam models with three and four holes are considered. Acceleration signals obtained from transverse vibration experiments are decomposed into intrinsic mode functions (IMFs) using the VMD method. Among the decomposed IMFs, those within the target frequency ranges considering the mechanical characteristics of simplified and complex systems are selected and transformed into frequency response functions (FRFs). These FRFs are roughly classified through the nonlinear transformation process, and it has become possible to interpret the complex system as the simplified system. The transformed signals are then used to generate virtual spectrograms, which are subsequently employed for training and validation in the deep residual network. In the first and second examples, looseness conditions are detected with accuracies of 95 % and 92 %, respectively, when using

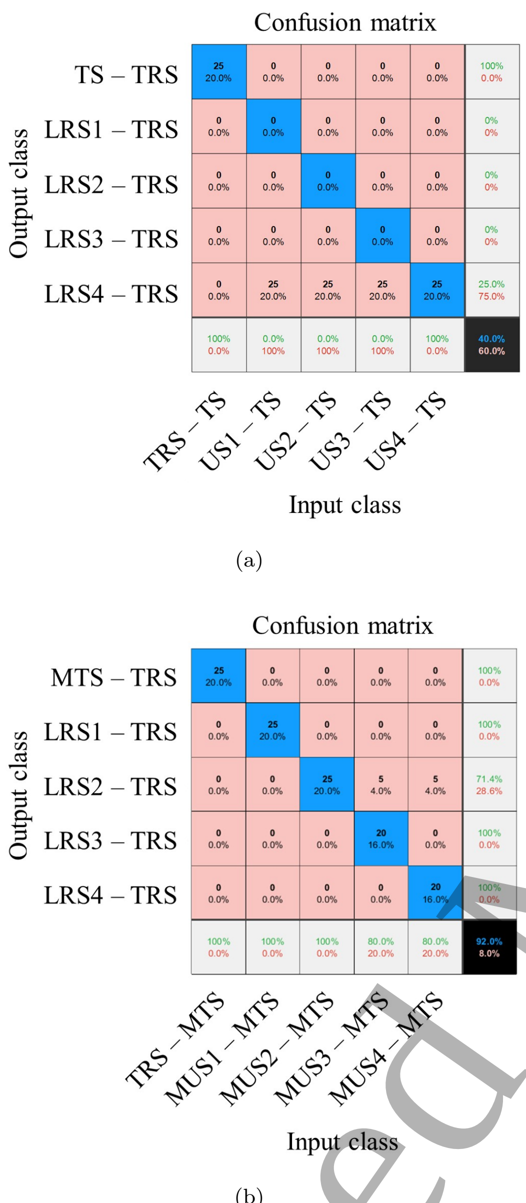

Figure 20. Confusion matrices showing the results of the looseness detection of the complex beam models with four holes. (a) The confusion matrix without the VMD-based NT method and (b) the confusion matrix with the VMD-based NT method.

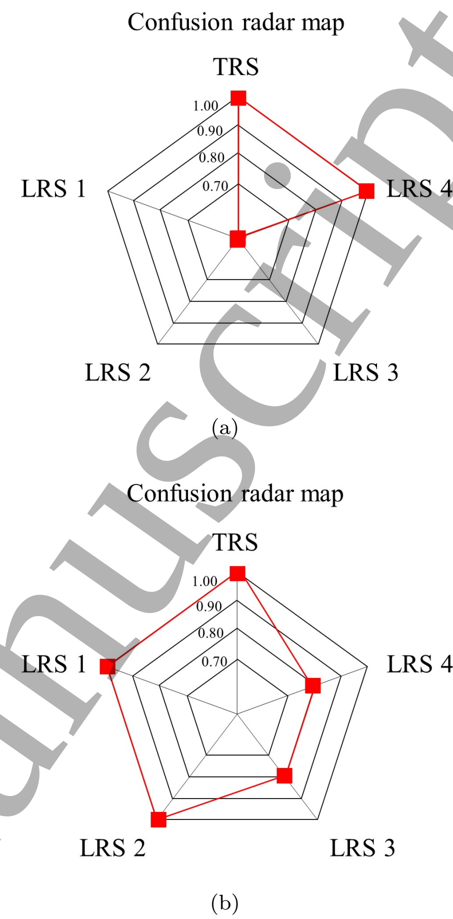

Figure 21. Confusion radar maps about the results of the confusion matrices. (a) The confusion radar map without the VMD-based NT method and (b) the confusion radar map with the VMD-based NT method.

the VMD-based NT method integrated with the deep residual network. In contrast, accuracies drop to 70 % and 40 % without the VMD-based NT method. By combining VMD and NT methods, effective signal processing and high accuracy are achieved, and the looseness conditions of bolted joints can be successfully detected. In the present study, structures with 3 or 4 bolts are employed, but structures with fewer than 3 or more than 4 bolts might be considered in future research. Moreover, the other assembly methods can be considered and the detection methods of multiple irregular signals of more complex structures in high-frequency bands can be developed.

5. Acknowledgment

This research was supported by the MOTIE (Ministry of Trade, Industry, and Energy) in Korea, under the Human Resource Development Program for Industrial Innovation(Global) (P0017306, Global Human Resource Development for Innovative Design in Robot and Engineering) supervised by the Korea Institute for Advancement of Technology (KIAT).

6. Declaration of conflicting interests

The author(s) declared no potential conflicts of interest with respect to the research, authorship, and/or publication of this article.

References

[1] JM Nichols, ST Trickey, M Seaver, SR Motley, and ED Eisner. Using ambient vibrations to detect loosening of a composite-to-metal bolted joint in the presence of strong temperature fluctuations. 2007.

[2] Francesco Amerini, Ettore Barbieri, Michele Meo, and Umberto Polimeno. Detecting loosening/tightening of clamped structures using nonlinear vibration techniques. *Smart materials and structures*, 19(8):085013, 2010.

[3] Feblil Huda, Itsuro Kajiwara, Naoki Hosoya, and Shozo Kawamura. Bolted joint loosening detection by using laser excitation. In *Health Monitoring of Structural and Biological Systems 2013*, volume 8695, pages 802–816. SPIE, 2013.

[4] Mengyang Zhang, Yanfeng Shen, Li Xiao, and Wenzhong Qu. Application of subharmonic resonance for the detection of bolted joint looseness. *Nonlinear dynamics*, 88:1643–1653, 2017.

[5] Pavlo Krot, Hamid Shiri, Przemysław Dabek, and Radosław Zimroz. Diagnostics of bolted joints in vibrating screens based on a multi-body dynamical model. *Materials*, 16(17):5794, 2023.

[6] Oybek Eraliev, Kwang-Hee Lee, and Chul-Hee Lee. Vibration-based loosening detection of a multi-bolt structure using machine learning algorithms. *Sensors*, 22(3):1210, 2022.

[7] Cheng Yuan, Shuyin Wang, Yanzhi Qi, and Qingzhao Kong. Automated structural bolt looseness detection using deep learning-based prediction model. *Structural Control and Health Monitoring*, 29(3):e2899, 2022.

[8] Joy Pal, Shirsendu Sikdar, and Sauvik Banerjee. A deep-learning approach for health monitoring of a steel frame structure with bolted connections. *Structural Control and Health Monitoring*, 29(2):e2873, 2022.

[9] Zhifeng Liu, Xing Yan, Wentao Chen, Nana Niu, Ming Li, and Ying Li. A prediction model of bolted joint loosening based on deep learning network. *Proceedings of the Institution of Mechanical Engineers, Part C: Journal of Mechanical Engineering Science*, page 09544062231202581, 2023.

[10] Nam-Gyu Park and Youn-sik Park. Identification of damage on a substructure with measured frequency response functions. *Journal of Mechanical Science and Technology*, 19:1891–1901, 2005.

[11] Aiko Furukawa, Hisanori Otsuka, and Junji Kiyono. Structural damage detection method using uncertain frequency response functions. *Computer-Aided Civil and Infrastructure Engineering*, 21(4):292–305, 2006.

[12] C Zang, Michael I Friswell, and M Imregun. Structural health monitoring and damage assessment using measured frfs from multiple sensors, part i: The indicator of correlation criteria. *Key Engineering Materials*, 245:131–140, 2003.

[13] Seong-Gyu Sim, Yeon-Jun Woo, Dong-Yoon Kim, Se Jin Hwang, Kyu Tae Hwang, Chang-Hun Lee, and Gil Ho Yoon. Experimental study of the effect of the boundary conditions of fractured bone. *Journal of the Mechanical Behavior of Biomedical Materials*, 124:104801, 2021.

[14] Gil Ho Yoon, Yeon-Jun Woo, Seong-Gyu Sim, Dong-Yoon Kim, and Se Jin Hwang. Investigation of bone fracture diagnosis system using transverse vibration response. *Proceedings of the Institution of Mechanical Engineers, Part H: Journal of Engineering in Medicine*, 235(5):597–611, 2021.

[15] Nam-Gyu Park and Youn-sik Park. Identification of damage on a substructure with measured frequency response functions. *Journal of Mechanical Science and Technology*, 19(10):1891–1901, 2005.

[16] S Rani, AK Agrawal, and V Rastogi. Vibration analysis for detecting failure mode and crack location in first stage gas turbine blade. *Journal of Mechanical Science and Technology*, 33:1–10, 2019.

[17] Young-Shin Lee and Myung-Jee Chung. A study on crack detection using eigenfrequency test data. *Computers & structures*, 77(3):327–342, 2000.

[18] J-M Ndambi, Johnny Vantomme, and Kristof Harri. Damage assessment in reinforced concrete beams using eigenfrequencies and mode shape derivatives. *Engineering structures*, 24(4):501–515, 2002.

[19] Dror Armon, Yakov Ben-Haim, and Simon Braun. Crack detection in beams by rankordering of eigenfrequency shifts. *Mechanical Systems and Signal Processing*, 8(1):81–91, 1994.

[20] Georgios I Giannopoulos. Crack identification in graphene using eigenfrequencies. *International Journal of Applied Mechanics*, 9(01):1750009, 2017.

[21] Hansang Kim and Hani Melhem. Damage detection of structures by wavelet analysis. *Engineering structures*, 26(3):347–362, 2004.

[22] SS Law, XY Li, XQ Zhu, and Siu Lai Chan. Structural damage detection from wavelet packet sensitivity. *Engineering structures*, 27(9):1339–1348, 2005.

[23] Wei Teng, Xian Ding, Shiyao Tang, Jin Xu, Bingshuai Shi, and Yibing Liu. Vibration analysis

for fault detection of wind turbine drivetrains—a comprehensive investigation. *Sensors*, 21(5):1686, 2021.

[24] Tianyang Wang, Qinkai Han, Fulei Chu, and Zhipeng Feng. Vibration based condition monitoring and fault diagnosis of wind turbine planetary gearbox: A review. *Mechanical Systems and Signal Processing*, 126:662–685, 2019.

[25] D Siano and MA Panza. Diagnostic method by using vibration analysis for pump fault detection. *Energy Procedia*, 148:10–17, 2018.

[26] Joan R Casas and John James Moughty. Bridge damage detection based on vibration data: past and new developments. *Frontiers in Built Environment*, 3:4, 2017.

[27] Paulo JS Cruz and Rolando Salgado. Performance of vibration-based damage detection methods in bridges. *Computer-Aided Civil and Infrastructure Engineering*, 24(1):62–79, 2009.

[28] Hao Liu, Dongliang Zuo, and Kun Zhang. Damage location diagnosis of urban rail transit bridge based on vehicle-induced vibration responses. In *IOP Conference Series: Materials Science and Engineering*, volume 592, page 012126. IOP Publishing, 2019.

[29] Le Wang, Zhichun Yang, and TP Waters. Structural damage detection using cross correlation functions of vibration response. *Journal of Sound and Vibration*, 329(24):5070–5086, 2010.

[30] Andreas Klausen and Kjell G Robbersmyr. Cross-correlation of whitened vibration signals for low-speed bearing diagnostics. *Mechanical Systems and Signal Processing*, 118:226–244, 2019.

[31] Xiaomin Zhao, Tejas H Patel, and Ming J Zuo. Multivariate emd and full spectrum based condition monitoring for rotating machinery. *Mechanical Systems and Signal Processing*, 27:712–728, 2012.

[32] Jacek Dybała and Radosław Zimroz. Rolling bearing diagnosing method based on empirical mode decomposition of machine vibration signal. *Applied Acoustics*, 77:195–203, 2014.

[33] Hua Li, Tao Liu, Xing Wu, and Qing Chen. An optimized vmd method and its applications in bearing fault diagnosis. *Measurement*, 166:108185, 2020.

[34] Jimeng Li, Xing Cheng, Qiang Li, and Zong Meng. Adaptive energy-constrained variational mode decomposition based on spectrum segmentation and its application in fault detection of rolling bearing. *Signal Processing*, 183:108025, 2021.

[35] Yanxue Wang, Richard Markert, Jiawei Xiang, and Weiguang Zheng. Research on variational mode decomposition and its application in detecting rub-impact fault of the rotor system. *Mechanical Systems and Signal Processing*, 60:243–251, 2015.

[36] Huan Zhou and Hao Wang. A study on fault diagnosis of rotating machinery combined wavelet transform with vmd. In *Journal of Physics: Conference Series*, volume 1626, page 012136. IOP Publishing, 2020.

[37] Hong Lu, Wei Zhang, Zhimin Chen, Zhangjie Li, Yongquan Zhang, Minghui Yang, and Chao Zou. Rotating machinery early fault detection integrating variational mode decomposition and multi-scale singular value decomposition. *Measurement Science and Technology*, 35(12):126128, 2024.

[38] Long Zhao, Guanru Wen, Zhicheng Liu, Yan Du, Jin Li, and Xinbo Huang. Method for extracting the free vibration response of transmission tower. *Measurement Science and Technology*, 35(2):025017, 2023.

[39] Junning Li, Wenguang Luo, and Mengsha Bai. Review of research on signal decomposition and fault diagnosis of rolling bearing based on vibration signal. *Measurement Science and Technology*, 2024.

[40] Xintian Chi, Dario Di Maio, and Nicholas AJ Lieven. Health monitoring of bolted joints using modal-based vibrothermography. *SN Applied Sciences*, 2:1–22, 2020.

[41] Feblil Huda, Itsuro Kajiwara, Naoki Hosoya, and Shozo Kawamura. Bolt loosening analysis and diagnosis by non-contact laser excitation vibration tests. *Mechanical Systems and Signal Processing*, 40(2):589–604, 2013.

[42] K He and WD Zhu. Detecting loosening of bolted connections in a pipeline using changes in natural frequencies. *Journal of Vibration and Acoustics*, 136(3):034503, 2014.

[43] Chao Xu, Chen-Chen Huang, and Wei-Dong Zhu. Bolt loosening detection in a jointed beam using empirical mode decomposition–based nonlinear system identification method. *International Journal of Distributed Sensor Networks*, 15(9):1550147719875656, 2019.

[44] Kyung-Young Jhang, Hai-Hua Quan, Job Ha, and Noh-Yu Kim. Estimation of clamping force in high-tension bolts through ultrasonic velocity measurement. *Ultrasonics*, 44:e1339–e1342, 2006.

[45] Sanat Wagle and Hiroshi Kato. Ultrasonic detection of fretting fatigue damage at bolt joints of aluminum alloy plates. *International Journal of Fatigue*, 31(8-9):1378–1385, 2009.

[46] Salim Chaki, Gilles Corneloup, Ivan Lillamand, and Henri Walaszek. Combination of longitudinal and transverse ultrasonic waves for in situ control of the tightening of bolts. 2007.

[47] Sopon Ritdumrongkul, Masato Abe, Yozo Fujino, and Takeshi Miyashita. Quantitative health monitoring of bolted joints using a piezoceramic actuator–sensor. *Smart materials and structures*, 13(1):20, 2003.

[48] Lin Chen, Haibei Xiong, Ziqian Yang, Youwei Long, Yewei Ding, and Qingzhao Kong. Preload measurement of steel-to-timber bolted joint using piezoceramic-based electromechanical impedance method. *Measurement*, 190:110725, 2022.

[49] Amin Baghalian, Volkan Y Senyurek, Shervin Tashakori, Dwayne McDaniel, and Ibrahim N Tansel. A novel nonlinear acoustic health monitoring approach for detecting loose bolts. *Journal of Nondestructive Evaluation*, 37:1–9, 2018.

[50] Francesco Amerini and Michael Meo. Structural health monitoring of bolted joints using linear and nonlinear acoustic/ultrasound methods. *Structural health monitoring*, 10(6):659–672, 2011.

[51] SK Samantaray, SK Mittal, P Mahapatra, and S Kumar. An impedance-based structural health monitoring approach for looseness identification in bolted joint structure. *Journal of Civil Structural Health Monitoring*, 8:809–822, 2018.

[52] Whitney D Reynolds, Derek Doyle, and Brandon Arritt. Active loose bolt detection in a complex satellite structure. In *Health Monitoring of Structural and Biological Systems 2010*, volume 7650, pages 117–130. SPIE, 2010.

[53] Seyed Majid Yadavar Nikravesh and Masoud Goudarzi. A review paper on looseness detection methods in bolted structures. *Latin American Journal of Solids and Structures*, 14(12):2153–2176, 2017.

[54] Yang Zhou, Hongzhen Yi, Xiaoyun Yue, Ang Li, Bin Hao, Xianfeng Yan, and Yitao Zhao. Method for loose bolt positioning and prediction of bolt axial force in bolt group. *Measurement*, 227:114316, 2024.

[55] Lingxiao Lu, Sancong Ying, Qian Xiao, and Chaohuan Hou. Bolt loosening status classification via waveenergy dissipation measurements withtemperature-compensated deep learning bypiezoelectric active sensing. *Measurement Science and Technology*, 2024.

[56] Long-Chao Chen, Yong-Zheng Jiang, Lei Huang, and Li-Ying Zeng. Monitoring method of bolt looseness based on inversion of joint surface gap by magnetic field change. *Measurement Science and Technology*, 34(8):085905, 2023.

[57] Geonkyo Hong and Dongjun Suh. Supervised-learning-based intelligent fault diagnosis for mechanical equipment. *IEEE Access*, 9:116147–116162, 2021.

[58] Guoqiang Li, Jun Wu, Chao Deng, Meirong Wei, and Xuebing Xu. Self-supervised learning for intelligent fault diagnosis of rotating machinery with limited labeled data. *Applied Acoustics*, 191:108663, 2022.

[59] Sang-Yun Lee and Sang-Kwon Lee. Deep convolutional neural network with new training method and transfer learning for structural fault classification of vehicle instrument panel structure. *Journal of Mechanical Science and Technology*, 34(11):4489–4498, 2020.

[60] Jeong Jun Lee, Deok Young Cheong, Tae Hong Min, Dong Hee Park, and Byeong Keun Choi. Cnn-based fault classification considered fault location of vibration signals. *Journal of Mechanical Science and Technology*, 37(10):5021–5029, 2023.

[61] Jae-Hong Lee, Do-Hyung Kim, Seong-Nyum Jeong, and Seong-Ho Choi. Detection and diagnosis of dental caries using a deep learning-based convolutional neural network algorithm. *Journal of dentistry*, 77:106–111, 2018.

[62] Parul Sharma, Yash Paul Singh Berwal, and Wiqas Ghai. Performance analysis of deep learning cnn models for disease detection in plants using image segmentation. *Information Processing in Agriculture*, 7(4):566–574, 2020.

[63] Xiaoli Zhao and Minping Jia. A novel unsupervised deep learning network for intelligent fault diagnosis of rotating machinery. *Structural Health Monitoring*, 19(6):1745–1763, 2020.

[64] Dong-Yoon Kim, EunBin Park, KyoBeom Ku, Se Jin Hwang, Kyu Tae Hwang, Chang-Hun Lee, and Gil Ho Yoon. Application of stacked autoencoder for identification of bone fracture. *Journal of the Mechanical Behavior of Biomedical Materials*, 146:106077, 2023.

[65] Tariq Mahmood, Jianqiang Li, Yan Pei, Faheem Akhtar, Suhail Ashfaq Butt, Allah Ditta, and Sirajuddin Qureshi. An intelligent fault detection approach based on reinforcement learning system in wireless sensor network. *The Journal of Supercomputing*, 78(3):3646–3675, 2022.

[66] Ruixin Wang, Hongkai Jiang, Zhenghong Wu, Jun Xu, and Jianjun Zhang. A reinforcement transfer learning method based on a policy gradient for rolling bearing fault diagnosis. *Measurement Science and Technology*, 33(6):065020, 2022.

[67] Zhewen Zhang and Lifeng Wu. Graph neural network-based bearing fault diagnosis using granger causality test. *Expert Systems with Applications*, 242:122827, 2024.

[68] Lu Xiao, Xiaoxin Yang, and Xiaodong Yang. A graph neural network-based bearing fault detection method. *Scientific Reports*, 13(1):5286, 2023.

[69] Konstantin Dragomiretskiy and Dominique Zosso. Variational mode decomposition. *IEEE transactions on signal processing*, 62(3):531–544, 2013.

[70] Jimeng Li, Xing Cheng, Qiang Li, and Zong Meng. Adaptive energy-constrained variational mode decomposition based on spectrum segmentation and its application in fault detection of rolling bearing. *Signal Processing*, 183:108025, 2021.

[71] Pinghe Ni, Jun Li, Hong Hao, Yong Xia, Xiangyu Wang, Jae-Myung Lee, and Kwang-Hyo Jung. Time-varying system identification using variational mode decomposition. *Structural Control and Health Monitoring*, 25(6):e2175, 2018.

[72] Dong-Yoon Kim, Yeon-Jun Woo, Keonwook Kang, and Gil Ho Yoon. Failure diagnosis system using a new nonlinear mapping augmentation approach for deep learning algorithm. *Mechanical Systems and Signal Processing*, 172:108914, 2022.

[73] Dong-Yoon Kim, Yeon-Jun Woo, Seong-Gyu Sim, and Gil Ho Yoon. Delamination diagnosis system using nonlinear transformation-based augmentation approach for cnn transfer learning. *Journal of Vibration Engineering & Technologies*, pages 1–18, 2023.

[74] Kaiming He, Xiangyu Zhang, Shaoqing Ren, and Jian Sun. Deep residual learning for image recognition. In *Proceedings of the IEEE conference on computer vision and pattern recognition*, pages 770–778, 2016.

[75] Saining Xie, Ross Girshick, Piotr Dollár, Zhuowen Tu, and Kaiming He. Aggregated residual transformations for deep neural networks. In *Proceedings of the IEEE conference on computer vision and pattern recognition*, pages 1492–1500, 2017.

[76] Anish Shah, Eashan Kadam, Hena Shah, Sameer Shinde, and Sandip Shingade. Deep residual networks with exponential linear unit. In *Proceedings of the third international symposium on computer vision and the internet*, pages 59–65, 2016.

[77] MATLAB. *Deep Learning Toolbox (R2023a)*. The MathWorks, Inc., Natick, Massachusetts, 2023.